VOLUME 116, NUMBER 11
JUNE 1, 1994

JOURNAL
OF THE
AMERICAN
CHEMICAL
SOCIETY

Enzymatic Reduction of Inorganic Anions. Variable-Temperature Steady-State and Pre-Steady-State Kinetics Experiments to Map the Energy Profile of an Enzymatic Multielectron Redox Reaction. Application to the Dissimilatory Sulfite Reductase from *Desulfovibrio vulgaris* (Hildenborough)

Siu Man Lui, Wen Liang, Aileen Soriano, and J. A. Cowan*

Contribution from Evans Laboratory of Chemistry, The Ohio State University, 120 West 18th Avenue, Columbus, Ohio 43210

Received November 11, 1993®

Abstract: Variable-temperature steady-state and pre-steady-state kinetics experiments have been carried out on the dissimilatory sulfite reductase (desulfoviridin) from *Desulfovibrio vulgaris* (Hildenborough). Activation free energies for reductive bond cleavage (ΔG_t^*) in SO_3^{2-}, NO_2^-, NO, and NH_2OH substrates have been evaluated from variable-temperature pre-steady-state kinetics data. Also, ground-state (ΔG_d) and transition-state (ΔG_t^*) contributions to the overall activation free energy (ΔG^*) have been determined from steady-state experiments. The choice of siroheme cofactor for this class of enzyme most likely reflects two factors underlying a preference for π-acceptor ligands. First, strong binding of substrate and weaker binding of product is promoted by the dominance of π-back-bonding. Second, population of an antibonding orbital in π-acceptor substrates lowers the transition-state contribution to the activation free energy and serves to weaken the chemical bond that is to be reductively cleaved. These conclusions are supported by quantitative evaluation of activation barriers for substrates and reaction intermediates.

Introduction

Enzyme-catalyzed reactions involving electron transfer to inorganic anions and gaseous molecules are key reaction pathways in respiratory and anabolic pathways in cellular metabolism.[1] Typically these reactions occur in a stepwise manner via a series of partially reduced intermediates.[2] To increase the mechanistic understanding of such reactions, our laboratory has initiated a series of studies to elucidate the molecular details of the chemistry underlying enzymatic nitrite and sulfite reduction. Recently we reported results from pre-steady-state kinetics experiments of enzymatic reduction of sulfite and nitrite catalyzed by a sulfite reductase (desulfoviridin) from the sulfate reducing bacterium *Desulfovibrio vulgaris* (Hildenborough).[3] The enzyme contains the coupled $[Fe_4S_4]$-siroheme prosthetic center common to this

* Abstract published in *Advance ACS Abstracts,* May 1, 1994.

(1) (a) Orme-Johnson, W. H. *Annu. Rev. Biophys. Biophys. Chem.* **1985**, *14*, 419–459. (b) Seefeldt, L. C.; Morgan, T. V.; Dean, D. R.; Mortenson, L. E. *J. Biol. Chem.* **1992**, *267*, 6680–8. (c) Madden, M. S.; Paustian, T. D.; Ludden, P. W.; Shah, V. K. *J. Bacteriol.* **1991**, *173*, 5403–5. (d) Higuchi, Y.; Yasuoka, N.; Kakudo, M.; Katsube, Y.; Yagi, T.; Inokuchi, H. *J. Biol. Chem.* **1987**, *262*, 2823–2826.

(2) (a) Tan, J.; Cowan, J. A. *Biochemistry* **1991**, *30*, 8910–8917. (b) Averill, B. A.; Tiejde, J. M. *FEBS Lett.* **1982**, *138*, 8–12. (c) Larsen, R. W.; Pan, L.-L.; Musser, S. M.; Li, Z.; Chan, S. I. *Proc. Natl. Acad. Sci. U.S.A.* **1992**, *89*, 723–727. (d) Chan, S. I.; Li, P. M. *Biochemistry* **1990**, *29*, 1–12. (e) Shapleigh, J. P.; Hosler, J. P.; Tecklenburg, M. M. J.; Kim, Y.; Babcock, G. T.; Gennis, R. B.; Ferguson-Miller, S. *Proc. Natl. Acad. Sci. U.S.A.* **1992**, *89*, 4786–4790.

(3) Lui, S. M.; Soriano, A.; Cowan, J. A. *J. Am. Chem. Soc.* **1993**, *115*, 10483–10486.

0002-7863/94/1516-4531$04.50/0

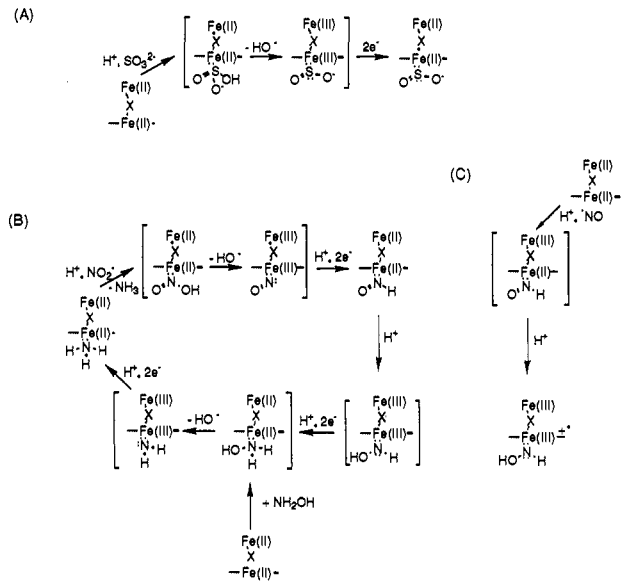

Figure 1. Summary of a working model for enzymatic reduction of oxidized sulfur and nitrogeneous substrates catalyzed by $[Fe_4S_4]$-siroheme centers: (A) profile for the first step of SO_3^{2-} reduction; (B) proposed reaction scheme for NO_2^- reduction; (C) reaction scheme for reduction of nitric oxide radical by the two-electron reduced enzyme. See ref 3 for additional details.

Table 1. Summary of Reaction Rate Constants at Room Temperature[3,4c]

	substrate			
	SO_3^{2-}	NO_2^-	NO	NH_2OH
$k_r(s^{-1})$[3]	12	14	6.5	9
$k_{cat}(s^{-1})$[4c]	0.3	0.04		30

class of sulfite and nitrite reductases.[4] Sulfite-reducing enzymes are capable of reducing nitrogenous substrates (NO_2^- or NH_2OH to NH_3), which are often more convenient for detailed mechanistic studies since NH_2OH is an intermediate state of the NO_2^- reduction pathway ($NO_2^- \rightarrow \rightarrow NH_2OH \rightarrow NH_3$).

Recently we reported results from a pre-steady-state kinetics analysis of the enzymatic reduction of SO_3^{2-}, NO_2^-, and subsequent putative intermediates.[3] The model for the reaction pathway is summarized in Figure 1, which shows enzymatic reduction arising through a sequence of three two-electron reductive cleavages of X–O bonds (X = S or N). By comparing the steady-state k_{cat} values with pre-steady-state rate constants for bond cleavage reactions (k_r), it is clear that only in the case of the intermediate species NH_2OH does $k_{cat} \sim k_r$ (Table 1), suggesting rate-limiting bond cleavage. The structural and stereoelectronic factors that control this reaction, differentiate substrates and intermediates, and promote substrate binding and catalytic activation are unclear. This lack of detailed mechanistic insight is generally valid for the broad spectrum of oxido-reductase enzymes required for electron transfer to substrate anions and gaseous molecules.

In addition to the bond cleavage step, the activation barriers for each step of the reaction reflect contributions from binding, steric barriers from protein side chains, and conformational motion of the protein backbone. Evaluation of these discrete contributions to the activation energy and understanding their relative magnitudes for a variety of substrate molecules represent a significant challenge. The availability of kinetics methods to monitor both steady- and pre-steady-state rate profiles for a number of substrates and reaction intermediates afforded us the opportunity to address this problem in quantitative detail. In this paper we report results from variable-temperature experiments conducted under steady-state and pre-steady-state conditions that account for the activation energies at each stage of the multistep reduction reaction. The free energy profiles resulting from this analysis offer insight on the catalytic mechanism and the importance of the special siroheme cofactor for mediating this reaction pathway.

Experimental Methods

General Materials and Instruments. Buffer salts were of molecular biology grade (Fisher or Aldrich Chemical Co.). Sephadex G-200 gel filtration material was obtained from Sigma, and DE-52 ion exchange resin, from Whatman. Deazaflavin was synthesized according to published protocols.[5]

Culture Growth/Protein Isolation and Purification. Desulfoviridin was isolated and purified from *Desulfovibrio vulgaris* (Hildenborough, NCIB 8303) using procedures described elsewhere.[3,4c]

Steady-State Kinetics. Kinetic data were obtained at 298 K by monitoring the decrease in absorbance at 600 nm of the $MeV^{+\bullet}$ radical anion used as an electron source for the enzyme during turnover. Aliquots of enzyme and substrate were added to a septum-stoppered glass cuvette that contained a volume (1.5–1.8 mL) of argon-purged potassium phosphate buffer (50 mM, pH 7.6). Actual concentrations of enzyme and substrate used in specific experiments are reported in the table footnotes. The resulting solution was further purged with oxygen-free argon for an additional 20 min. A volume of a $MeV^{+\bullet}$ stock solution was added to give an initial $A_{600} \sim 2.5$ ($\epsilon_{600nm} = 1.3 \times 10^4$ cm^{-1} M^{-1})[6] in a total working volume of 2 mL. The $MeV^{+\bullet}$ stock was prepared by zinc reduction of MeV^{2+}. Acid-washed zinc granules were reacted with 35 mg of methyl viologen hydrochloride in 8 mL of argon-purged potassium phosphate (50 mM, pH 7.6). Kinetic measurements were made by following the initial rate of change of the absorbance monitored at 600 nm. To inhibit nonenzymatic reduction of nitrite by $MeV^{+\bullet}$, sodium diethyldithiocarbamate (25 μM) was included in nitrite-containing mixtures. The resulting decay profile was analyzed using software from On-Line Instruments Systems. Michaelis–Menten parameters were determined using commercially available software (Origin).

Pre-Steady-State Kinetics. A 10-mL volume of a solution containing 60 μM enzyme, 120 μM deazaflavin, and 15 mM EDTA in potassium phosphate buffer (50 mM, pH 7.6) was deaerated in a 10-mL pear-shaped flask by purging the surface of the stirred solution for 30 min with O_2-free Ar(g). A gas-tight Hamilton syringe was preflushed with Ar(g) and loaded with the Ar(g)-purged solution under positive pressure. The syringe mouth was fitted with a small serum stopper to prevent O_2 diffusion and subsequently immersed in ice water and irradiated (1000-W lamp, 90% power) for 20 min to promote deazaflavin photoreduction of DV.[7] During preliminary experiments, reduction was monitored by electronic absorption spectroscopy and irradiation was continued until no further change was observed in the optical spectrum. A second gas-tight syringe was loaded in the same manner with the appropriate argon-purged substrate solution (see footnote to Table 5), without subsequent irradiation. The stopped-flow apparatus was flushed with Ar(g)-purged buffer prior to each experiment. Reactants in the drive syringes were preequilibrated at the appropriate temperature prior to mixing, and absorption changes were typically monitored at 438 nm. During the course of the experiment, the gas-tight Hamilton syringe containing the enzyme was irradiated for 2 min to ensure retention of a high fraction of the two-electron reduced enzyme during the prolonged experiments. A water filter was placed between the syringe and the lamp.

Data were obtained with an OLIS (On-Line Instrument Systems, Inc.) stopped-flow apparatus as previously described.[3] Rate constants were determined by use of the OLIS Operating System software (version 12.05) by fitting to proprietary software for rise–fall kinetics.

Results

To delineate the energy profile for the multistep redox reaction catalyzed by the dissimilatory sulfite reductase, we have examined

(4) (a) Cowan, J. A.; Sola, M. *Inorg. Chem.* **1990**, *29*, 2176–2179. (b) Christner, J. A.; Munck, E.; Janick, P. A.; Siegel, L. M. *J. Biol. Chem.* **1983**, *258*, 11147–11156. (c) Wolfe, B. M.; Lui, S. M.; Cowan, J. A. *Eur. J. Biochem.* **1994**, in press.

(5) Janda, M.; Hemmerich, P. *Angew. Chem., Int. Ed. Engl.* **1976**, *15*, 443–444.

(6) Thorneley, R. N. F. *Biochim. Biophys. Acta* **1974**, *333*, 487–496.

(7) Massey, V.; Hemmerich, P. *Biochemistry* **1978**, *17*, 9–17.

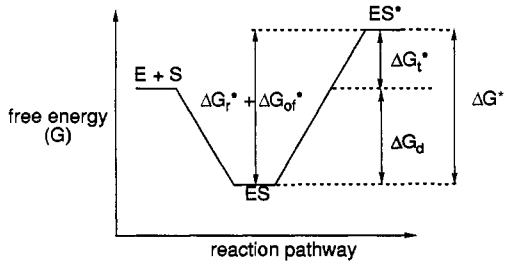

Figure 2. General free energy profiles for substrate turnover showing the components of ΔG_r^*, ΔG_{of}^*, ΔG_d, and ΔG_t^*. Specific data are listed in Tables 2–5.

the temperature dependence of both steady-state and pre-steady-state kinetic rate constants. The latter principally reflect bond cleavage chemistry, while the former also reflect additional activation barriers on the reaction pathway. Moreover, only for the pre-steady-state study (and also the steady-state kinetics of hydroxylamine reduction) can we investigate individual two-electron reductive bond cleavage steps along the reaction pathway. That is, steady-state turnover data obtained for SO_3^{2-} or NO_2^- reduction include the complete sequence of three two-electron reductive steps.

Steady-State Variable-Temperature Data. Our initial studies have shown that the steady-state kinetics of the reaction can be reasonably considered in terms of a Michaelis–Menten model. In this model k_{cat} reflects transition-state energies and K_m reflects ground-state binding energies.[8] The assumption that $K_m \sim K_d$ (to a reasonable approximation) appears justified inasmuch as the K_m's determined for substrates are very similar to K_d's evaluated for inhibitor analogues (CN^- and HS^-), while the likely error range would influence neither the discussion nor conclusions presented below.[11] For steady-state turnover, several simple relationships between standard parameters (k_{cat} and K_m) and activation energies are readily derived, where ΔG_d and ΔG_t^* are the ground- and transition-state contributions to the activation free energy (ΔG^*) (Figure 2). These profiles can be developed more thoroughly by including the analysis of the temperature dependence of pre-steady-state rates (discussed below) since each discrete bond breaking step can be independently studied. The magnitude of ΔG^* can be directly determined at any temperature from eq 1, which can be rewritten in the form of (2), where k,

$$k_{cat} = (kT/h) \exp -(\Delta G^*/RT) \quad (1)$$

$$R \ln(k_{cat}h/kT) = \Delta S^* - \Delta H^*/T \quad (2)$$

R, and h are the Boltzmann, gas, and Planck constants, respectively. The latter equation was used to evaluate the values of ΔH^* and ΔS^* (Table 2) from the temperature dependence of k_{cat} and plots directly analogous to those shown in Figure 3.

The transition-state contribution (ΔG_t^*) to the activation free energy (ΔG^*) can be estimated in a similar fashion from $\ln(k_{cat}/K_m) - \ln(kT/h)$ (eq 3a), and the enthalpic and entropic components, from the temperature dependence defined by eq 3b. For each substrate, the temperature dependence of K_m was evaluated and the appropriate value was used. Estimates of ΔG_d are made from relationship 5, assuming $K_m \sim K_d$.

$$RT \ln(k_{cat}/K_m) = RT \ln(kT/h) - \Delta G_t^* \quad (3a)$$

$$R \ln[(k_{cat}h)/(K_m kT)] = \Delta S_t^* - \Delta H_t^*/T \quad (3b)$$

$$\Delta G^* = \Delta G_t^* + \Delta G_d \quad (4)$$

$$\Delta G_d = -RT \ln K_m \quad (5)$$

Figure 3 illustrates typical plots obtained from variable-temperature steady-state experiments by use of eqs 2 and 3b, respectively. The activation parameters thereby determined are listed in Tables 2–4. Overall, there is a general decrease in the magnitude of ΔG^* from SO_3^{2-} and NO_2^- to NH_2OH. This arises not through a decrease in the magnitude of ΔG_t^*, which in fact increases over this series, but rather through a decrease in the magnitude of ΔG_d, reflecting stronger binding by the π-acceptor ligands NO_2^- and SO_3^{2-}. The lower ΔG_t^* values for these π-acceptor ligands presumably arise through population of the antibonding N–O (or S–O) orbitals, which weakens the bond toward reductive cleavage.[9]

Pre-Steady-State Variable-Temperature Data. The temperature dependence of the Arrhenius rate constant k_r is given by eq 6, which can be rewritten in the form of (7) that is of greater

$$k_r = kT/h \exp -(\Delta G_r^*/RT) \quad (6)$$

$$R \ln(k_r h/kT) = \Delta S_r^* - \Delta H_r^*/T \quad (7)$$

utility for variable-temperature experiments since it accounts for the inherent temperature dependence of ΔG_r^*. This form of the rate equation has been used to analyze pre-steady-state rate data. Figure 4 illustrates typical plots obtained from variable-temperature stopped-flow data using eq 7. The activation free energy (ΔG_r^*) is calculated directly from eq 6, and the enthalpic (ΔH_r^*) and entropic (ΔS_r^*) components, from the temperature dependence of k_r defined by eq 7. The results from these measurements are given in Table 5. We will consider first the data for the family of nitrogenous substrates before commenting later on the result for sulfite. The free activation barrier (ΔG_r^*) for two-electron reduction of nitrite (16.2 kcal mol^{-1}) is similar to that for nitrous oxide (16.0 kcal mol^{-1}) but differs from the value for hydroxylamine (14.9 kcal mol^{-1}). There is, however, a more systematic change in the enthalpic and entropic components, which is discussed in a later section. In particular we observe a decrease in the magnitude of the enthalpic barrier for the more reduced substrates, which may correlate with substrate bond energy, and also an increase in the entropic barrier.

Discussion

In previous work we have demonstrated a small apparent k_{cat} for SO_3^{2-} and NO_2^- relative to that for NH_2OH reduction (Table 1), suggesting that bond cleavage steps in the early stages of the reaction might be rate-limiting. This would follow expectations based on the relative S–O and N–O bond energies for each substrate. This is, the resonance-stabilized sulfite and nitrite anions react more slowly than hydroxylamine. However, this hypothesis is not supported by the similarity in rate constants for bond cleavage determined from pre-steady-state kinetic measurements for two-electron reductions of SO_3^{2-}, NO_2^-, NO, and NH_2OH [$k_r(SO_3^{2-}) \sim 12$ s^{-1}, $k_r(NO_2^-) \sim 14$ s^{-1}, $k_r(NO) \sim 6.5$ s^{-1},

(8) Fersht, A. *Enzyme Structure and Mechanism*; Freeman: New York, 1985.

(9) Jolly, W. L. *Modern Inorganic Chemistry*; McGraw-Hill: New York, 1984; pp 365–370, 438–444.

(10) Isaacs, N. S. *Physical Organic Chemistry*; Longman: New York, 1987, p 102.

(11) Substrate or ligand anions of similar bonding capabilities appear to have similar binding affinities. For example, compare $K_m(SO_3^{2-}) \sim 59$ μM with $K_d(CN^-) \sim 200$ μM, and $K_m(NH_2OH) \sim 59$ mM with $K_d(HS^-) \sim 21$ mM (Liang and Cowan, unpublished results). Minor systematic errors in K_d will have no effect on the conclusions reached in our discussion of the data, while major discrepancies are unlikely. A 10-fold error in K_d introduces an error of 1.4 kcal mol^{-1} in ΔG_d. Since $K_d \leq K_m$, only if the magnitude of K_d for NH_2OH is underestimated by $\sim$4 kcal mol^{-1} (that is, by 10^3-fold) are the general conclusions compromised. The on-rate for NH_2OH has previously been determined ($\sim$24 M^{-1} s^{-1})[1,3] and so an off-rate of $\sim 1.2 \times 10^{-3}$ s^{-1} would be required for a binding affinity in the 50 μM range. This is inconsistent with estimates of off-rates for related ligands [$k_{off}(NH_3) \geq 30$ s^{-1} and $k_{off}(HS^-) \geq 0.3$ s^{-1}; Liang and Cowan, unpublished results, and ref 3] and suggests that K_d for NH_2OH will not be significantly smaller than $K_m(NH_2OH)$.

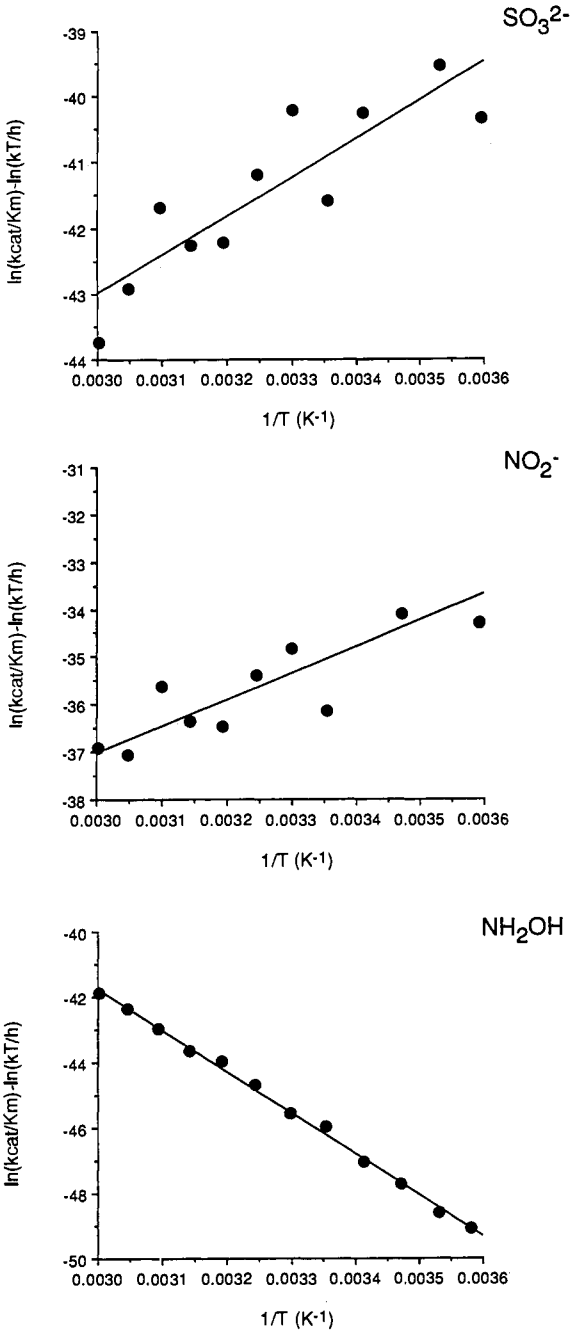

Figure 3. Steady-state data. Plot of $R \ln[(k_{cat}h)/(K_m kT)]$ versus $1/T$ for a variety of substrate molecules. Enthalpic and entropic components (ΔH_t^* and ΔS_t^*) were obtained from the slope and intercept according to eq 3b.

and $k_r(NH_2OH) \sim 9\ s^{-1}$].[3] This dichotomy can be explained if the π-acid ligands SO_3^{2-} and NO_2^- should exhibit weaker S–O and N–O bonds, respectively, after binding to the electron-rich siroheme as a result of π-back-bonding and population of the antibonding S–O and N–O orbitals. In this paper, we have described a series of experiments that lend quantitative support to this hypothesis and construct a free energy profile for the catalytic reduction of NO_2^- to NH_3. This provides considerable insight on the factors underlying the enzymatic reduction of these inorganic species.

Activation Parameters. For NO_2^-, SO_3^{2-}, and NO reduction, we have demonstrated through pre-steady-state kinetic measurements that k_{cat} does not reflect reductive bond cleavage,[3] and so the activation parameters noted in Figure 2 for NO_2^- reduction include other factors (ΔG_{of}^*) that so far remain ill-defined. That is, the $\Delta G^*(NO_2^-)$ indicated in Figure 2 contains contributions

Table 2. Steady-State Activation Parameters[a]

substrate	ΔH^* (kcal mol^{-1})	ΔS^* (cal K^{-1} mol^{-1})	ΔG^* (kcal mol^{-1})
SO_3^{2-}	2.6	−51.7	18.0
NO_2^-	−6.8	−79.8	17.0
NH_2OH	3.1	−41.3	15.4

[a] Kinetics data were obtained as previously described using saturating concentrations of substrate and $MeV^{+\bullet}$.[4c] Samples were incubated for 15 min at the appropriate temperature, over the range 10–45 °C, before the addition of $MeV^{+\bullet}$. Reaction conditions were as follows: [DV] = 140 nM, $[SO_3^{2-}]$ = 1 mM, $[NO_2^-]$ = 200 μM, $[NH_2OH]$ = 150 mM. The activation free energy at 298 K was determined directly from eq 1, and the enthalpic and entropic components were determined from eq 2. Errors in each measurement are estimated to be on the order of ±0.5 kcal mol^{-1} for ΔH^*, $\pm 2K^{-1}$ cal mol^{-1} for ΔS^*, and ±0.2 kcal mol^{-1} for ΔG^*. Any temperature dependence of the constant K_m was accounted for over the temperature range employed. Nitric oxide proved to be unsuitable as a substrate for steady-state kinetics experiments.

Table 3. Breakdown of Steady-State Activation Parameters[a]

substrate	ΔH_t^* (kcal mol^{-1})	ΔS_t^* (cal K^{-1} mol^{-1})	ΔG_t^* (kcal mol^{-1})
SO_3^{2-}	−5.8	−60.5	12.2
NO_2^-	−5.6	−53.8	10.4
NH_2OH	12.6	−3.9	13.8

[a] Kinetics data were obtained as described in the legend to Table 2. The activation free energy at 298 K was determined directly from eq 3a, and the enthalpic and entropic components were determined from eq 3b. Errors in each measurement are estimated to be on the order of ±0.5 kcal mol^{-1} for ΔH_t^*, ±2 cal K^{-1} mol^{-1} for ΔS_t^*, and ±0.2 kcal mol^{-1} for ΔG_t^*.

Table 4. Summary of the Factors Contributing to the Activation Free Energy[a]

substrate	ΔG_r^*	ΔG_{of}^*	ΔG^*	ΔG_t^*	ΔG_d (kcal mol^{-1})
SO_3^{2-}	15.6	2.4	18.0	12.2	5.8
NO_2^-	16.2	0.8	17.0	10.4	6.6
NO	16.0		≤17.0	~1.9 (est)	~14.1 (est)
NH_2OH	14.9	0.5	15.4	13.8	1.6

[a] All data are in units of kcal mol^{-1}. Kinetics parameters were determined from eqs 1–8 and using the data from Tables 2, 3, and 5. Errors in each measurement are estimated to be on the order of ±0.2 kcal mol^{-1}. Other than ΔG_r^*, data for NO have been estimated (see ref 12) owing to the problems associated with steady-state turnover of this reactive substrate.

Table 5. Pre-Steady-State Bond Cleavage Data[a]

substrate	ΔH_r^* (kcal mol^{-1})	ΔS_r^* (cal K^{-1} mol^{-1})	ΔG_r^* (kcal mol^{-1})
SO_3^{2-}	12.2	−11.4	15.6
NO_2^-	17.4	4.0	16.2
NO	12.5	−11.9	16.0
NH_2OH	5.0	−33.1	14.9

[a] Stopped-flow kinetics of data for substrates were obtained as previously described by monitoring the change in absorbance at 438 nm.[3] The solution conditions are detailed as follows: [DV] = 30 μM, $[SO_3^{2-}]$ = 50 mM, $[NO_2^-]$ = 50 mM, [NO] = 1 mM, $[NH_2OH]$ = 100 mM. Parameters were determined from eq 6 and 7 presented in the text. Samples were incubated for 15 min at the appropriate temperature over the range 8–45 °C prior to mixing. Errors in each measurement are estimated to be on the order of ±0.3 kcal mol^{-1} for ΔH_r^*, ±1.5 cal K^{-1} mol^{-1} for ΔS_r^*, and ±0.4 kcal mol^{-1} for ΔG_r^*.

from both ΔG_r^* and ΔG_{of}^* (eq 8). The contribution to ΔG^*

$$\Delta G^*(NO_2^-) = \Delta G_r^*(NO_2^-) + \Delta G_{of}^*(NO_2^-) \qquad (8)$$

from bond cleavage (ΔG_r^*) can be independently determined from the pre-steady-state variable-temperature data for the two-electron reductions of NO_2^-, SO_3^{2-}, NO, and NH_2OH. Using the ΔG^* values determined from steady-state rate measurements, the additional contributions (ΔG_{of}^*) from enzyme conformational changes, etc., can be determined (Table 4). The results demonstrate that bond cleavage gives rise to the dominant barrier for enzymatic substrate reduction (that is, $\Delta G_r^* \gg \Delta G_{of}^*$). In

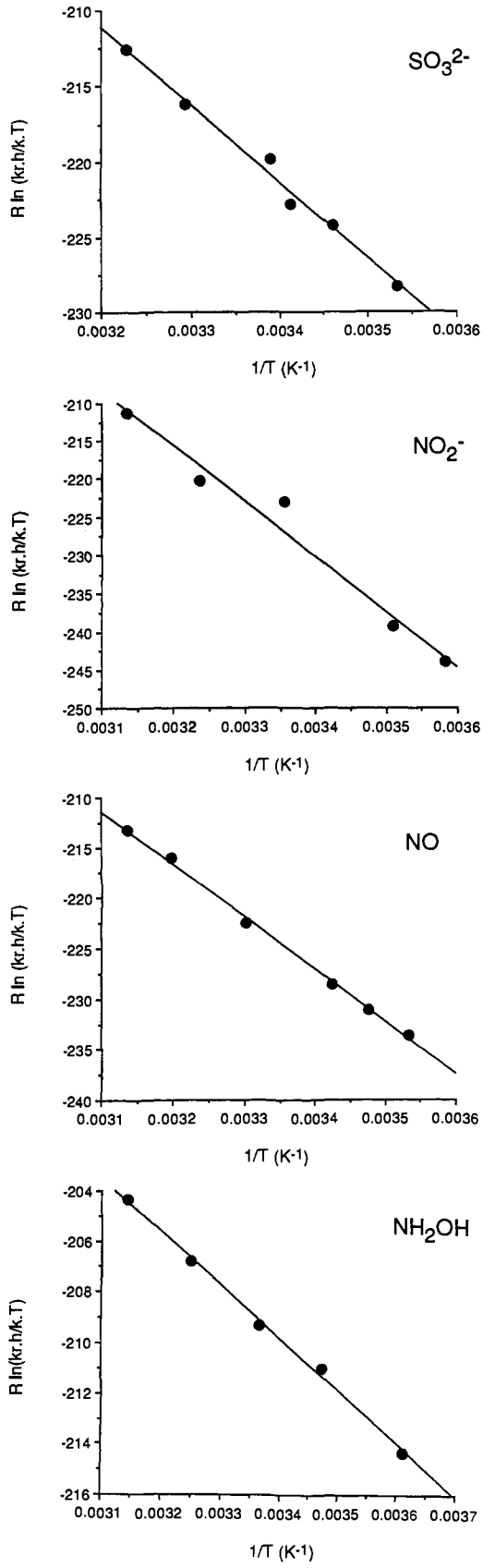

Figure 4. Pre-steady-state data. Plot of $R \ln(k_r h/kT)$ versus $1/T$ for a variety of substrate molecules. Enthalpic and entropic components (ΔH_r^* and ΔS_r^*) were obtained from the slope and intercept according to eq 7.

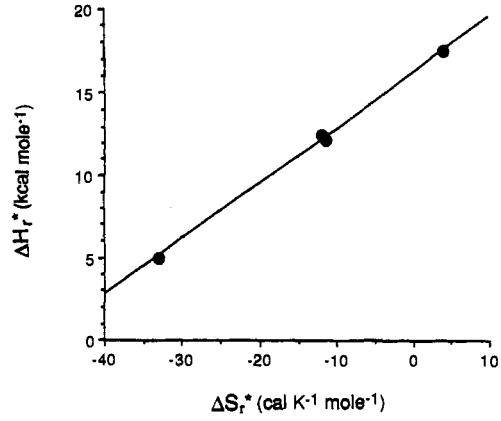

Figure 5. Isokinetic plot of ΔH_r^* versus ΔS_r^*. The gradient yields an isokinetic temperature of 334 K (correlation coefficient of 0.998). Data for SO_3^{2-}, NO_2^-, NO, and NH_2OH were taken from Table 5.

the specific case of hydroxylamine we might expect $\Delta G_{of}^*(NH_2OH) \sim 0$ since $k_{cat} \sim k_r$. It is therefore reassuring to note that this is indeed experimentally verified [$\Delta G^*(NH_2OH) \sim 15.4$ kcal mol^{-1}; $\Delta G_r^*(NH_2OH) \sim 14.9$ kcal mol^{-1}; $\Delta G_{of}^*(NH_2OH) \sim 0.5$ kcal mol^{-1}], confirming the conclusions reached earlier that bond cleavage is the dominant rate-limiting step for this substrate. For earlier reaction intermediates there is apparently a significant contribution from ΔG_{of}^* (but much smaller than ΔG_r^*). The origin of this barrier remains unclear at this time but may involve conformational changes of the protein or siroheme ring. Figure 2 and Tables 2–5 summarize our current evaluation of the free energy profiles that can be constructed from this data.

For a series of similar reactions there can exist a linear relationship between the activation enthalpies and entropies.[10] By writing the free energy change (ΔG^*) in a revised form ($\Delta H^* = T\Delta S^* + \Delta G^*$), it is seen that a linear plot of ΔH^* versus ΔS^* (obtained from variable-temperature studies on a family of related reactions) yields a temperature T (isokinetic temperature) at which the Arrhenius plots for each data set would intersect. In theory such a linear relationship suggests the dominance of one stereoelectronic parameter in controlling the relative rates of a number of substrates.[10] The isokinetic relationship also reflects a balancing of the change in one activation parameter by another. That is, a more negative enthalpic component is offset by a more negative entropic component, and vice versa. Figure 5 shows the isokinetic plot obtained from the variation of ΔH_r^* and ΔS_r^*, which yielded an isokinetic temperature of 334 K (correlation coefficient of 0.998). As noted earlier, there is a general decrease in the magnitude of ΔH_r^*, which most likely reflects the difference in bond energies. Since related plots for ΔH^* versus ΔS^* and ΔH_t^* versus ΔS_t^* are obtained over a narrower range of values, the deviations from experimental error are more pronounced but the general trends are similar.

Implications for Understanding the Reaction Mechanism. In the discussion that follows, emphasis will be placed on the enzymatic reduction of NO_2^- to NH_3 rather than the reaction of SO_3^{2-}. This simply reflects the availability of reaction intermediates and substrate analogues for the former with which to carry out detailed kinetics studies. It is reasonable to assume that the arguments and conclusions presented below are equally valid for SO_3^{2-} reduction. We also note that there is an implicit assumption that the magnitude of ΔG^* for any given substrate mainly reflects the activation barrier for the first two-electron reductive cleavage. That is, ΔG^* for NO_2^- reflects the first two-electron step for $NO_2^- \rightarrow$ "NO^-", etc., rather than reduction of a later intermediate. We feel that this is justified inasmuch as there is a decrease in the magnitude of ΔG^* moving from NO_2^- to NH_2OH as the substrate (see the note in ref 12 for the special case of nitric oxide).

For nitric oxide, only the magnitude of ΔG_r^* could be determined experimentally. However, estimates of ΔG^*, ΔG_t^*,

and ΔG_d could be readily evaluated, as described in ref 12. The following trends in activation free energies may be noted from the data in Tables 2–4. First, the magnitude of ΔG^* decreases as $SO_3^{2-} > NO_2^- \sim NO > NH_2OH$. Second, ΔG_t^* increases, with SO_3^{2-} and $NO_2^- < NH_2OH$. Third, the binding affinity ΔG_d varies as SO_3^{2-} and $NO_2^- > NH_2OH$. Note that NO yields anomalous ΔG_t^* and ΔG_d values as a result of the unusually strong binding to siroheme (see ref 12). In the discussion that follows we will show how the observed trends in free energy components lend considerable insight on the design of the catalytic site and, in particular, the choice of siroheme as the catalytic cofactor.

Role of the Siroheme Cofactor. The general decrease in ΔG_d over the series SO_3^{2-} and NO_2^- to NH_2OH reflects the change in bonding as we progress from the strong π-acceptors SO_3^{2-} and NO_2^- to the σ-donor NH_2OH. We have noted elsewhere how the electron-rich siroheme ring has a particularly high affinity for π-acceptor ligands.[3] We shall now argue that the bonding mode that results in tight binding by NO_2^- is also responsible for the reversal in the relative magnitudes of ΔG_t^* along the same series. Population of the antibonding S–O and N–O orbitals as a result of π-back-bonding weakens the chemical bonds that are to be reductively cleaved.[9] This is reflected in the smaller values of ΔG_t^* for SO_3^{2-} and NO_2^- relative to the corresponding parameter for NH_2OH (Table 4). We see then that the relative magnitudes of the ΔG_d and ΔG_t^* components are in opposition with regard to defining the overall activation barrier ΔG^*. Although the absolute magnitude of the ΔG_t^* component is substantially greater than that of ΔG_d, the relative change in the magnitude of ΔG_d, comparing substrates and reaction intermediates, is larger than the corresponding change in the ΔG_t^* term. The observed trend in the magnitude of the ΔG^* values therefore reflects the dominance of the binding term (ΔG_d). The design of the prosthetic center therefore accomodates two important requirements: (1) Strong binding of the substrate and weaker binding of the product is promoted by the dominance of π-back-bonding. These factors are also manifest by the kinetic rate constants for release of the substrate and product.[3,4b] (2) The aforementioned scheme serves to weaken the chemical bond that is to be reductively cleaved by populating an antibonding orbital in π-acceptor substrates, thereby lowering the transition-state contribution to the activation free energy.[9] This is carried to an extreme in the case of nitric oxide (ref 12), although the intermediate (HNO) to be expected during nitrite turnover would most likely fit in with the overall trends noted above for ΔG^*, ΔG_d, and ΔG_t^* in the series $NO_2^- \rightarrow HNO \rightarrow NH_2OH \rightarrow NH_3$. We note that we have not discussed the contributions of proton-transfer steps, which appear to be rapid and do not contribute significantly to ΔG^*.

Summary. In this paper we have evaluated the component activation energies for each step of the catalytic reduction of an inorganic anion by variable-temperature experiments conducted under steady-state and pre-steady-state conditions. The free energy profiles resulting from the analysis offer insight on the catalytic mechanism and the importance of the special siroheme cofactor for mediating this reaction pathway. This strategy should be of general value for the analysis of multistep enzymatic reductions of other inorganic substrates. This represents part 2 of a detailed study of the structural and electronic features of the substrate and enzyme that control ground- and transition-state energies for enzyme-catalyzed reduction of inorganic anions.[14]

Acknowledgment. This work was supported by the NSF, Grant Number CHE-8921468. J.A.C. is a fellow of the Alfred P. Sloan Foundation and a National Science Foundation Young Investigator.

(12) The binding energy K_d may be estimated from k_{off}/k_{on}. We previously determined k_{on}(NO) $\sim 7 \times 10^5$ M^{-1} s^{-1}.[3] We have no estimate of k_{off} for the NO complex of desulfoviridin; however, Olson has reported $k_{off} \sim 3 \times 10^{-5}$ s^{-1} for binding to heme in the α- and β-subunits of hemoglobin.[13] Using this as an estimate yields $K_d \sim 4.3 \times 10^{-11}$ M (or $\Delta G_d \sim 14.1$ kcal mol^{-1} at 298 K). We have determined $\Delta G_r^* \sim 16$ kcal mol^{-1}. For π-accepting nitrogenous species, ΔG_{off}^* typically falls in the range of ~ 1 kcal mol^{-1} (Table 4). Use of the relevant forms of eqs 4 and 8 puts an upper limit of ca. 17 kcal mol^{-1} for ΔG^*, and so if $\Delta G_d \sim 14.1$ kcal mol^{-1} then $\Delta G_t^* \sim 1.9$ kcal mol^{-1}.

(13) Olson, J. S. *Methods Enzymol.* **1981**, *76*, 631–651.

(14) Part 1 of this work is described in ref 3.